© 2021. Published by The Company of Biologists Ltd | Development (2021) 148, dev191122. doi:10.1242/dev.191122

RESEARCH REPORT

HoxD transcription factors define monosynaptic sensory-motor specificity in the developing spinal cord

Fumiyasu Imai[1,2,3,*], Mike Adam[3], S. Steven Potter[3] and Yutaka Yoshida[1,2,3,*]

ABSTRACT

The specificity of monosynaptic connections between proprioceptive sensory neurons and their recipient spinal motor neurons depends on multiple factors, including motor neuron positioning and dendrite morphology, axon projection patterns of proprioceptive sensory neurons in the spinal cord, and the ligand-receptor molecules involved in cell-to-cell recognition. However, with few exceptions, the transcription factors engaged in this process are poorly characterized. Here, we show that members of the HoxD family of transcription factors play a crucial role in the specificity of monosynaptic sensory-motor connections. Mice lacking *Hoxd9*, *Hoxd10* and *Hoxd11* exhibit defects in locomotion but have no obvious defects in motor neuron positioning or dendrite morphology through the medio-lateral and rostro-caudal axes. However, we found that quadriceps motor neurons in these mice show aberrant axon development and receive inappropriate inputs from proprioceptive sensory axons innervating the obturator muscle. These genetic studies demonstrate that the HoxD transcription factors play an integral role in the synaptic specificity of monosynaptic sensory-motor connections in the developing spinal cord.

KEY WORDS: Axon guidance, Motor neuron, Proprioceptive sensory neuron, Sensory-motor circuit, Spinal cord, Synaptic specificity, Mouse

INTRODUCTION

Proprioceptive sensory pathways relay important information about the state of muscle contraction to motor neurons in the spinal cord (Arber, 2012; Catela et al., 2015; Imai and Yoshida, 2018; Zampieri and Nooij, 2021). This enables motor coordination through the precise harmonization and orchestration of limb movements (Akay et al., 2014; Mayer et al., 2018; Santuz et al., 2019; Akay, 2020). Proprioceptive sensory neurons, which are located in the dorsal root ganglion (DRG), innervate muscle spindles and Golgi tendon organs in the periphery. In the spinal cord, proprioceptive sensory neurons and motor neurons project axons to the same or synergistic muscles to form monosynaptic connections, whereas they do not form monosynaptic connections when they project to antagonistic muscles (Ladle et al., 2007; Mendelsohn et al., 2015; Imai and Yoshida, 2018; Balaskas et al., 2020). The specificity of these monosynaptic sensory-motor connections has been suggested to be encoded genetically through coordinated regulation of motor pool positioning, motor neuron dendrite patterning, and the angular approaches of proprioceptor axons to their motor neuron dendrite targets. (Frank, 1990; Mendelson and Frank, 1991; Vrieseling and Arber, 2006; Sürmeli et al., 2011; Mendelsohn et al., 2015; Baek et al., 2017; Balaskas et al., 2019). Loss of transcription factor FoxP1, for example, affects motor pool locations and results in inappropriate sensory-motor connections (Sürmeli et al., 2011). In addition, another study demonstrates a strong correlation between monosynaptic sensory-motor specificity and the angles of proprioceptive sensory axons and directionality of motor neuron dendrites (Balaskas et al., 2019).

Several molecules involved in the finer facets of sensory-motor specificity have also been identified. The repellent signaling molecule, semaphorin 3E (Sema3E) has been shown to repel proprioceptive sensory axons expressing its receptor, plexin D1 (PlxnD1), thereby regulating sensory-motor specificity (Pecho-Vrieseling et al., 2009; Fukuhara et al., 2013). Inactivation of either *Sema3E* or *PlxnD1* causes defects in sensory-motor specificity without affecting either the positioning or dendritic development of motor neurons (Pecho-Vrieseling et al., 2009; Fukuhara et al., 2013). More recently, expression of Hoxc8 in proprioceptive sensory neurons has been shown to play a role in the monosynaptic sensory-motor specificity of particular forelimb sensory motor circuits, possibly by regulating gene expression in proprioceptive sensory neurons (Shin et al., 2020).

Transcription factors have well-documented roles in spinal cord development. The Hox family, for example, participates in regulating a wide range of developmental processes including rostro-caudal axis development, motor pool specification and guidance of skeletal and limb development (Dasen and Jessell, 2009; Jung et al., 2010; Lacombe et al., 2013; Philippidou and Dasen, 2013; Catela et al., 2015; Sweeney et al., 2018; Baek et al., 2019). Despite the various roles of Hox transcription factors in motor neuron patterning and specification, it remains unknown whether the expression of Hox transcription factors in motor neurons directly regulate monosynaptic sensory-motor specificity.

In this report, we examined whether HoxD transcription factors impact the development of monosynaptic sensory-motor specificity by focusing on the well-characterized quadriceps and obturator sensory-motor reflex circuit in the lumbar spinal cord (Mears and Frank, 1997). *Hoxd9* and *Hoxd10* are expressed in the lumbar spinal cord and locomotor deficits have been reported in *Hoxd10* single- and *Hoxd9, 10* double-mutant mice (Carpenter et al., 1997; de la Cruz et al., 1999; Tschopp et al., 2012). As there are many classes of Hox genes, the effects of deleting a single gene may be compensated for by other closely related members of the Hox family. To overcome this issue, *Hoxd9*, *10*, and *11* triple mutant mice have been generated (hereafter, *Hoxd9, 10, 11*$^{-/-}$; Raines et al., 2013). These triple mutant mice are documented to have

[1]Neural Connectivity Development in Physiology and Disease Laboratory, Burke Neurological Institute, White Plains, NY 10605, USA. [2]Feil Family Brain and Mind Research Institute, Weill Cornell Medicine, New York, NY 10065, USA. [3]Division of Developmental Biology, Cincinnati Children's Hospital Medical Center, Cincinnati, OH 45229, USA.

*Authors for correspondence (yoy4001@med.cornell.edu; fui4001@med.cornell.edu)

Y.Y., 0000-0003-0664-0888

Handling Editor: François Guillemot
Received 31 March 2020; Accepted 17 May 2021

Development (2021) 148, dev191122. doi:10.1242/dev.191122

defects in reproductive tract development (Raines et al., 2013), but the effects of *Hoxd9*, *Hoxd10*, and *Hoxd11* deletion on motor circuits and behavior are unknown. Thus, we tested the idea of compensatory functioning of multiple Hox proteins through an analysis of the quadriceps and obturator sensory-motor reflex circuit in *Hoxd9, 10, 11*$^{-/-}$ mice.

RESULTS AND DISCUSSION

Hoxd9, Hoxd10 and Hoxd11 are not essential for cell fate determination in quadriceps motor neurons

To determine whether HoxD transcription factors are involved in the assembly of sensory-motor reflex circuits, we first examined the expression patterns of *Hoxd9*, *Hoxd10* and *Hoxd11* in the mouse spinal cord, DRG and muscles. *Hoxd9* and *Hoxd10* were expressed in the rostral lumbar spinal cord (Fig. 1A,B; Fig. S1) as previously reported (Choe et al., 2006; Wu et al., 2008). *Hoxd11* was expressed in the caudal but not the rostral lumbar spinal cord (Fig. 1C; Fig. S1) (Davis and Capecchi, 1994; Tschopp et al., 2012). Expression of these three Hox genes was not detected in the DRG or the quadriceps muscles (Fig. 1A-F). *Hoxd10* was expressed in both spinal interneurons and motor neurons, with strong expression in Islet1^{off} lateral motor column (LMC) neurons (Fig. 1G,H) (Choe et al., 2006; Wu et al., 2008).

To assess the roles of Hoxd9, Hoxd10 and Hoxd11 in motor neuron development at lumbar levels, we analyzed the preganglionic column (PGC), hypaxial motor column (HMC), median motor column (MMC) and LMC (Fig. 1I-N,S,T) in *Hoxd9, 10, 11*$^{-/-}$ mice (Raines et al., 2013). Motor neurons from the PGC, HMC, MMC and LMC project their axons into sympathetic ganglia, hypaxial muscles, axial muscles and limb muscles, respectively. PGCs, identified by neuronal nitric oxide synthase (nNOS), were located in the thoracic spinal cord (Fig. 1I,Q), whereas HMC and MMC neurons were detected with Islet1 (Fig. 1I,K). Finally, LMC neurons at lumbar levels were identified by FoxP1 (Fig. 1M). Based on nNOS, Islet1 and FoxP1 immunohistochemistry, we observed no overt differences in the positioning or numbers of PGC, HMC/MMC or LMC motor neurons between control and *Hoxd9, 10, 11*$^{-/-}$ mice (Fig. 1I-N,Q,R). To further characterize LMC, Pea3^{on} motor neurons were analyzed. Pea3^{on} motor neurons were located in lateral LMC and projected into rectus femoris muscles, which is one of quadriceps muscles (Fig. 1O) (Arber et al., 2000). Pea3^{on} motor neurons were similarly segregated both in control and *Hoxd9, 10, 11*$^{-/-}$ mice (Fig. 1O,P). In addition, at lumbar levels, the number of Pea3^{on} motor neurons was similar between control and mutant embryos. (Fig. 1Q,R). We also assessed the expression of a motor neuron pool marker, *Sema3e*, which, at hindlimb levels, is expressed in gluteus motor neurons (Pecho-Vrieseling et al., 2009; Fukuhara et al., 2013), but we observed no differences in *Sema3e* expression between control and *Hoxd9, 10, 11*$^{-/-}$ mice (Fig. 1S,T).

Taken together, these data indicate that Hoxd9-11 transcription factors are not necessary for general motor column or motor pool patterning within the thoracic and lumbar spinal cord during mouse development.

Specification of quadriceps and obturator motor neurons

To determine whether Hoxd9-11 transcription factors influence monosynaptic sensory-motor specificity, we examined the motor neurons that innervate the quadriceps and obturator muscles as the monosynaptic sensory-motor specificity within this muscle pair has been well-characterized at lumbar levels (Mears and Frank, 1997). To assess cell body positions and dendritic morphologies of the quadriceps and obturator motor neurons, we employed a viral retrograde labeling approach. We injected AAV6-CAG-tdTomato into the quadriceps and obturator (gracilis) muscles at postnatal day (P) 3 mice and analyzed them at P10 (Fig. 2A-D). First, we examined cell body positions along the medio-lateral axis of the lumbar spinal cord. In P10 wild-type mice, quadriceps and obturator motor neurons were located laterally (60.5±6.8% of motor neurons were located 600-800 µm from the midline; mean±s.d.) and medially (72.2±14.8% of motor neurons were 0-600 µm from the midline), respectively (Fig. 2E,G). Similar distributions of motor neurons were observed in *Hoxd9, 10, 11*$^{-/-}$ mice (Fig. 2F,H; quadriceps: 64.4±17.1% of motor neurons were 600-800 µm from the midline, P=0.32; obturator: 74.1±16.0% of motor neurons were 0-600 µm from the midline, P=0.85). Motor neuron cell body positions along the rostro-caudal axis were also similar between wild-type and mutant mice (Fig. 2I,J; distance from L1 for quadriceps motor neurons in wild type: 1555±207 µm, mutants: 1556±233 µm; distance from L1 for obturator motor neurons in wild-type: 1219±267 µm, mutants: 1185±321 µm). Thus, proper quadriceps and obturator motor neuron positions were maintained in *Hoxd9, 10, 11*$^{-/-}$ mice.

As motor neuron dendrite morphology has been shown to affect synaptic specificity between proprioceptors and their appropriate spinal motor neuron targets (Vrieseling and Arber, 2006; Balaskas et al., 2019), we subsequently analyzed the dendritic arborization patterns of quadriceps and obturator motor neurons. Radial plot analyses of the densities of motor neuron dendrites or of dendrites and cell bodies combined showed similar arched dendrite distributions for quadriceps and obturator motor neurons in wild-type and *Hoxd9, 10, 11*$^{-/-}$ mice (Fig. 2K-T). This strongly suggests that loss of Hoxd9-11 does not affect dendrite development or patterning in quadriceps and obturator motor neurons.

Hoxd9-11 transcription factors are involved in axonal projections of motor neurons

As previous studies have suggested that retrograde signals from muscles to motor neurons and proprioceptive sensory neurons influence sensory-motor circuit specificity (Haase et al., 2002; Vrieseling and Arber, 2006; Wang et al., 2007), we then examined the axonal projections of quadriceps and obturator motor neurons to their cognate muscle targets using *Hb9-GFP* reporter mice, in which GFP is expressed in motor neurons (Wichterle et al., 2002; De Marco Garcia and Jessell, 2008). At embryonic day (E) 15.5, motor nerves projecting to quadriceps (vasti and rectus femoris) muscles were thinner and less branched in *Hoxd9, 10, 11*$^{-/-}$ mice compared with wild-type mice (Fig. 2U,V) (axon volume: wild-type, 100±26%; mutants, 40±16%; P<0.01, n=4, see Materials and Methods for details). In contrast, we detected no obvious differences in the obturator nerves between control and *Hoxd9, 10, 11*$^{-/-}$ mice (Fig. 2W,X) (wild-type, 100±11%; mutants, 99±14%; P=0.87, n=4). These data indicate that Hoxd9-11 transcription factors are crucial for quadriceps, but not obturator motor axon projections and branches.

Hoxd9-11 transcription factors regulate specificity of monosynaptic sensory-motor connections

To determine whether there were any functional defects in the synaptic specificity of monosynaptic sensory-motor connections in *Hoxd9, 10, 11*$^{-/-}$ mice, we performed intracellular recordings from both quadriceps and obturator motor neurons after peripheral nerve stimulation in P5-P7 mice (Fig. 3A) (Mears and Frank, 1997). We identified the quadriceps and obturator motor neurons by virtue of their antidromic responses to electrical stimuli applied to their

Development (2021) 148, dev191122. doi:10.1242/dev.191122

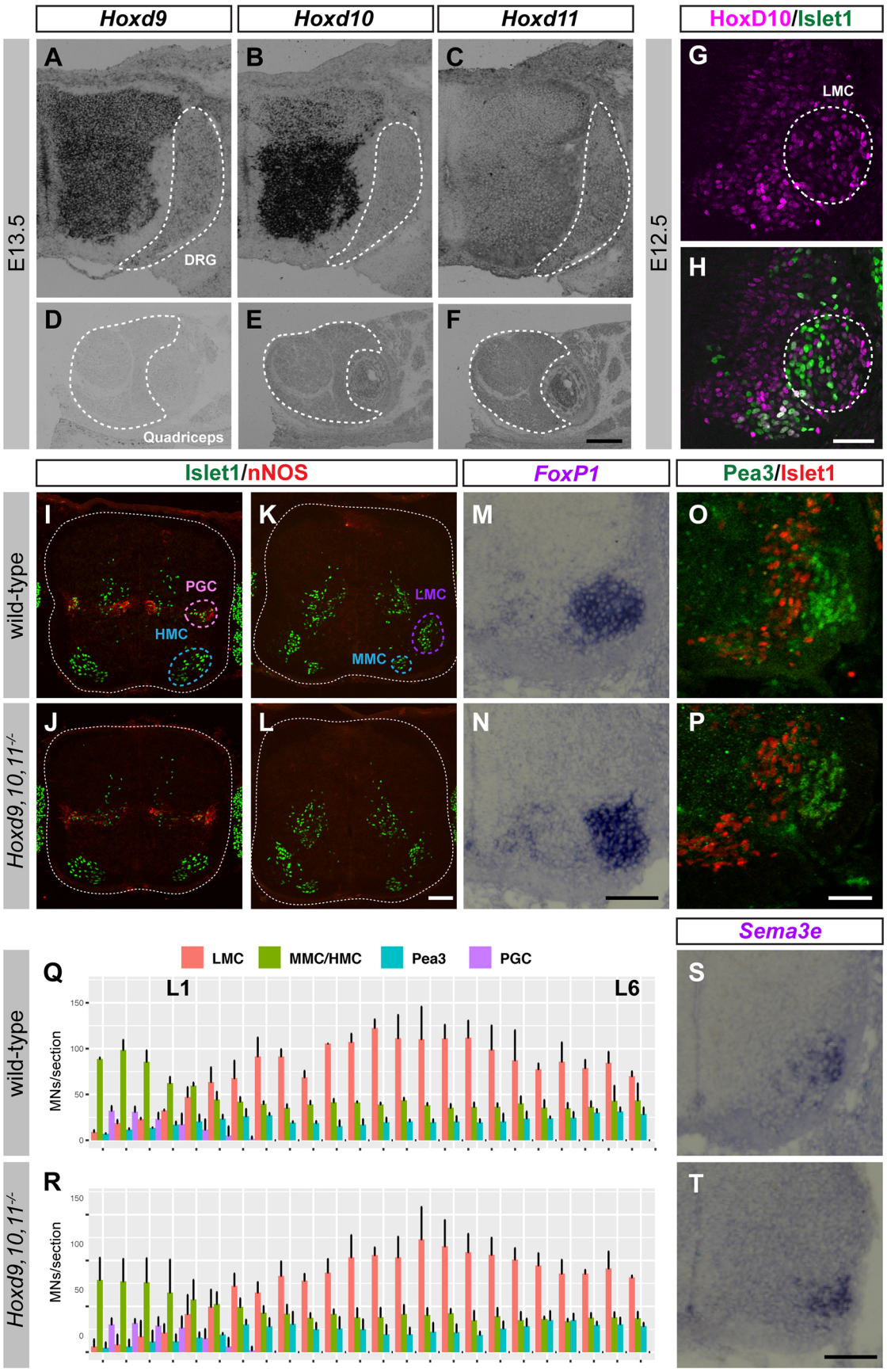

Fig. 1. See next page for legend.

Development (2021) 148, dev191122. doi:10.1242/dev.191122

Fig. 1. Inactivation of *HoxD9*, *HoxD10 and HoxD11* does not disturb motor neuron differentiation along the rostro-caudal axis of the lumbar spinal cord. (A-F) *In situ* hybridization of *Hoxd9* (A,D), *Hoxd10* (B,E) and *Hoxd11* (C,F) in the spinal cord and dorsal root ganglion (DRG) (A-C) and quadriceps muscles (D-F) in E13.5 wild-type embryos. Dotted lines indicate the boundaries of the DRGs (A-C) and quadriceps muscles (D-F). (G,H) Immunostaining of HoxD10 (magenta) and Islet1 (green) at E12.5. Dotted lines delineate the lateral motor column. (I-P) Labeling of Islet1 (green) and nNOS (red) (I-L), *FoxP1* (M,N), and Pea3 (green) and Islet1 (red) (O,P) in wild-type (I,K,M,O) and *Hoxd9, 10, 11*$^{-/-}$ (J,L,N,P) embryos at E13.5. (Q,R) Quantification of motor neurons per section (L1-L6). Data are mean±s.d. (n=4). (S,T) Labeling of *Sema3e* in wild-type (S) and *Hoxd9, 10, 11*$^{-/-}$ (T) embryos at E13.5. Scale bars: 100 µm.

respective muscle nerves. After detection of antidromic responses, motor responses to other stimulated muscle nerves were recorded. We found no aberrant antidromic responses in either wild-type or *Hoxd9, 10, 11*$^{-/-}$ mice (quadriceps motor neurons, wild type=0/13, mutants=0/15; obturator motor neurons, wild type=0/8, mutants=0/13), indicating that quadriceps and obturator motor neurons project appropriately to their target muscles. To identify the latencies of monosynaptic sensory-motor connections, we analyzed the homonymous connections of obturator and quadriceps sensory-motor circuits in wild-type mice. Latencies of monosynaptic connections following obturator and quadriceps nerve stimulation ranged between 4.41 to 5.89 ms and 3.96 to 5.98 ms, respectively (red dotted lines in Fig. 3D,E; see Materials and Methods for details). To determine the specificity of monosynaptic sensory-motor connections, excitatory postsynaptic potentials (EPSPs) and shortest latencies were recorded from quadriceps motor neurons with obturator nerve stimulation (Fig. 3B-D). Intriguingly, we found aberrant monosynaptic connections between obturator sensory nerves and quadriceps motor neurons in *Hoxd9, 10, 11*$^{-/-}$ mice (wild-type: 0/13, mutants: 6/15, Fig. 3D, right panel). We also analyzed obturator motor neurons with quadriceps nerve stimulation; however, we found no monosynaptic connections in either control or *Hoxd9, 10, 11*$^{-/-}$ mice (wild-type: 0/8, mutants: 0/13, Fig. 3E, right panel). There were also no significant differences in homonymous EPSPs between wild-type and *Hoxd9, 10, 11*$^{-/-}$ mice (Ob-Ob wild-type: 4.78±2.70 mV, mutants: 3.50±2.44 mV, P=0.289; Q-Q wild-type: 5.79±2.44 mV, mutants: 3.96±2.94 mV, P=0.083, Fig. 3F left, middle). Monosynaptic EPSPs from quadriceps motor neurons after obturator sensory nerve stimulation in *Hoxd9, 10, 11*$^{-/-}$ mice were similar to homonymous quadriceps circuits in wild-type mice (4.63 ±2.96 mV, Fig. 3F right). Taken together, these results reveal that quadriceps motor neurons receive aberrant inputs from obturator sensory nerves in *Hoxd9, 10, 11*$^{-/-}$ mice (Fig. 3G).

What is the mechanism underlying synaptic specificity regulated by HoxD9-11 transcription factors? *Hoxd9, 10, 11*$^{-/-}$ mice showed no defects in motor neuron topography (Figs 2 and 3). Dendrite morphologies of quadriceps and obturator motor neurons in *Hoxd9, 10, 11*$^{-/-}$ mice were also identical to control mice. However, we found defects in peripheral projections of quadriceps but not obturator motor neurons in *Hoxd9, 10, 11*$^{-/-}$ mice, raising the possibility that retrograde signaling may be impaired between the quadriceps muscle and its innervating motor neurons. It is possible that the reduction in quadriceps motor axons in the quadriceps muscle may affect expression of signaling molecules or axon guidance molecules in the quadriceps motor neurons, and degrade monosynaptic sensory-motor specificity.

Hoxd9, 10, 11$^{-/-}$ mice exhibit defects in locomotion

To assess whether *Hoxd9, 10, 11*$^{-/-}$ mice have locomotor deficits, hindlimb joint angles were analyzed on a treadmill at 25 cm/s (Fig. 4A). *Hoxd9, 10, 11*$^{-/-}$ mice showed foot-dragging behaviors (red arrows in Fig. 4C) similar to what has been previously reported in *Hoxd9, d10* double-mutant mice (de la Cruz et al., 1999). In addition to altered toe trajectories, maximum and minimum joint angles of hindlimbs were also affected during locomotion in *Hoxd9, 10, 11*$^{-/-}$ mice (Fig. 4B). Minimum joint angles of hips and ankles (hips: wild-type, 79.4±8.7°, mutants, 61.8±7.2°; ankles: wild-type, 58.9±5.9°, mutants, 96.9±4.7°) and maximum joint angles of the knees and the metatarsal phalangeal joints (MTP) (knees: wild-type, 113.7±9.2, mutants, 95.4±9.3°; MTP: wild-type, 163.6±6.2°, mutants, 152.0±4.5°) were also affected during locomotion in *Hoxd9, 10, 11*$^{-/-}$ mice (Fig. 4B). No significant differences were observed in joint angles during the swing to stance transitions (Fig. 4D,E). Hip and knee angles were more flexed and ankle angles were extended during the transitions from stance to swing phases in *Hoxd9, 10, 11*$^{-/}$ mice (Fig. 4F,G). These results demonstrate that deletion of Hoxd9-11 caused changes in locomotor behaviors in terms of foot-dragging and altered joint angles during the transitions between the swing and stance phases of locomotion. Surprisingly, these locomotor defects in *Hoxd9, 10, 11*$^{-/-}$ mice appear to be milder than those observed in *Hoxd10* single- or *Hoxd9, 10* double-mutant mice (Carpenter et al., 1997; de la Cruz et al., 1999). This may be due to the different gene knockout strategies employed. Indeed, *Hoxd9, 10, 11*$^{-/-}$ mice do not show defects in hindlimb development, unlike *Hoxd10* single- or *Hoxd9, 10* double-mutant mice which show hindlimb skeletal abnormalities (Carpenter et al., 1997; de la Cruz et al., 1999; Raines et al., 2015). Moreover, as the behavioral deficits in *Hoxd9, 10, 11*$^{-/-}$ mice do not seem to simply be explained by defects in quadriceps and obturator sensory-motor circuits or through aberrant development of quadriceps motor axons, it is plausible that other sensory-motor circuits could be affected in *Hoxd9, 10, 11*$^{-/-}$ mice.

Although the precise mechanisms underlying Hoxd9-11-mediated sensory-motor specificity are not yet clear, this study has identified a group of transcription factors that can influence synaptic specificity in the developing monosynaptic sensory-motor circuit in the spinal cord. This study, along with previous studies (Fukuhara et al., 2013; Baek et al., 2017), suggests that transcriptional and repellent molecular programs contribute to the finer-grain aspects of sensory-motor specificity, and a delicate interaction between positional and molecular cues is likely necessary to achieve the highly complex neural circuit wiring seen in the mammalian central nervous system.

MATERIALS AND METHODS

Mice

The following mouse lines were used in this study: *Hoxd9, 10, 11*$^{-/-}$ (Raines et al., 2013) and *Hb9-GFP* (Wichterle et al., 2002). Mouse handling and procedures were approved by the Institutional Animal Care and Use Committee at the Cincinnati Children's Hospital Research Foundation and Burke Neurological Institute. We used wild-type litter mates as controls and both sexes were used for this study.

Behavioral analysis

After shaving the adult mice (2-3 months old), joints (hip, ankle, MTP) and the tips of digits (toes) were marked and recorded with a high-speed video camera (Blackfly S, 226fps, FLIR). Treadmill speed (Harvard Apparatus) was set to 25 cm/s after a 5-min warm up at 15 cm/s. Joint markers were tracked with DeepLabCut (Mathis et al., 2018; Nath et al., 2019) and marker positions and joint angles were analyzed using R statistical software (https://www.R-project.org/). Knee angles were calculated by triangulation with hip and ankle coordinates, as well as the lengths of femurs and tibias.

Development (2021) 148, dev191122. doi:10.1242/dev.191122

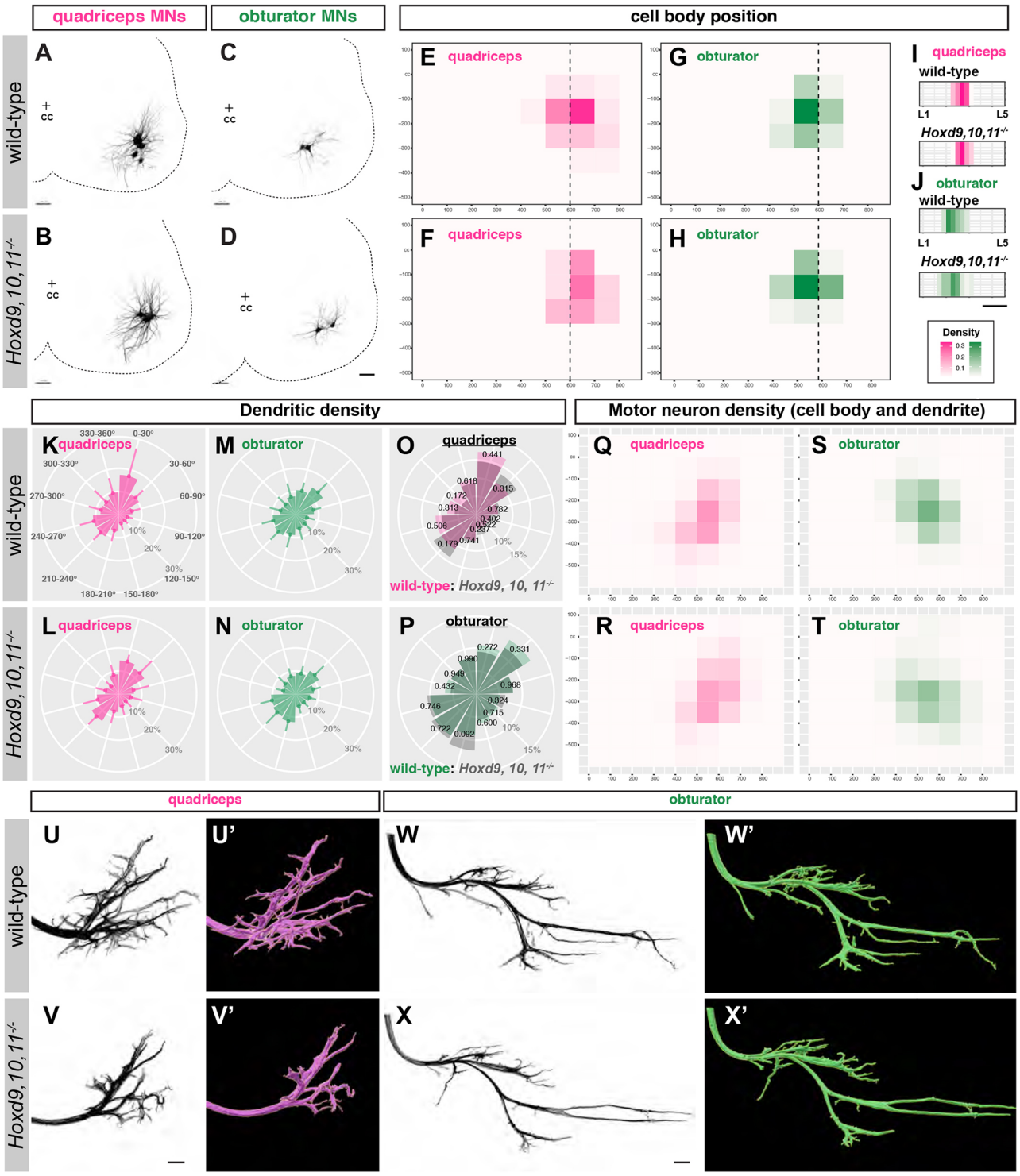

Fig. 2. HoxD9, HoxD10 and HoxD11 are not necessary for the location and dendritic development of quadriceps and obturator motor neurons. (A-D) Quadriceps (A,B) and obturator motor neurons (C,D) were retrogradely labeled in wild-type (A,C) and *Hoxd9, 10, 11*$^{-/-}$ (B,D) mice. cc, central canal. (E-H) Density plots of cell body positions from quadriceps (E,F) and obturator (G,H) motor neurons in wild-type (E,G) and *Hoxd9, 10, 11*$^{-/-}$ (F,H) mice. Bin size: 100 µm×100 µm with cc as the origin. Wild-type data: quadriceps (*n*=55, from four mice) and obturator (*n*=52, from five mice). *Hoxd9, 10, 11*$^{-/-}$ mouse data: quadriceps (*n*=50, from five mice) and obturator (*n*=51, from four mice). (I,J) Density plots of cell body positions from quadriceps (I) and obturator (J) motor neurons along the rostro-caudal axis. Bin size: 200 µm. (K-P) Dendritic densities of quadriceps (K,L) and obturator (M,N) motor neurons in wild-type (K,M) and *Hoxd9, 10, 11*$^{-/-}$ (L,N) mice were not significantly different (O-P, *P*-values are indicated). Wild-type data: quadriceps (*n*=15, from four mice) and obturator (*n*=15, from five mice). *Hoxd9, 10, 11*$^{-/-}$ mouse data: quadriceps (*n*=11, from five mice) and obturator (*n*=15, from four mice). (Q-T) Density plots of motor neurons (dendrites and cell bodies combined) from quadriceps (Q,R) and obturator motor neurons (S,T) in wild-type (Q,S) and *Hoxd9, 10, 11*$^{-/-}$ (R,T) mice. Bin size: 100 µm×100 µm from cc. Wild-type data: quadriceps (*n*=15, from four mice) and obturator (*n*=15, from five mice). *Hoxd9, 10, 11*$^{-/-}$ mouse data: quadriceps (*n*=11, from five mice) and obturator (*n*=15, from four mice). (U-X′) Hb9-positive quadriceps (U,V) and obturator (W,X) motor axons from wild-type (U,W) and *Hoxd9, 10, 11*$^{-/-}$ (V,X) embryos at E15.5. U′-X′ show three-dimensional reconstructions of motor axons. Scale bars: 100 µm (D,V,X); 1 mm (J).

Development (2021) 148, dev191122. doi:10.1242/dev.191122

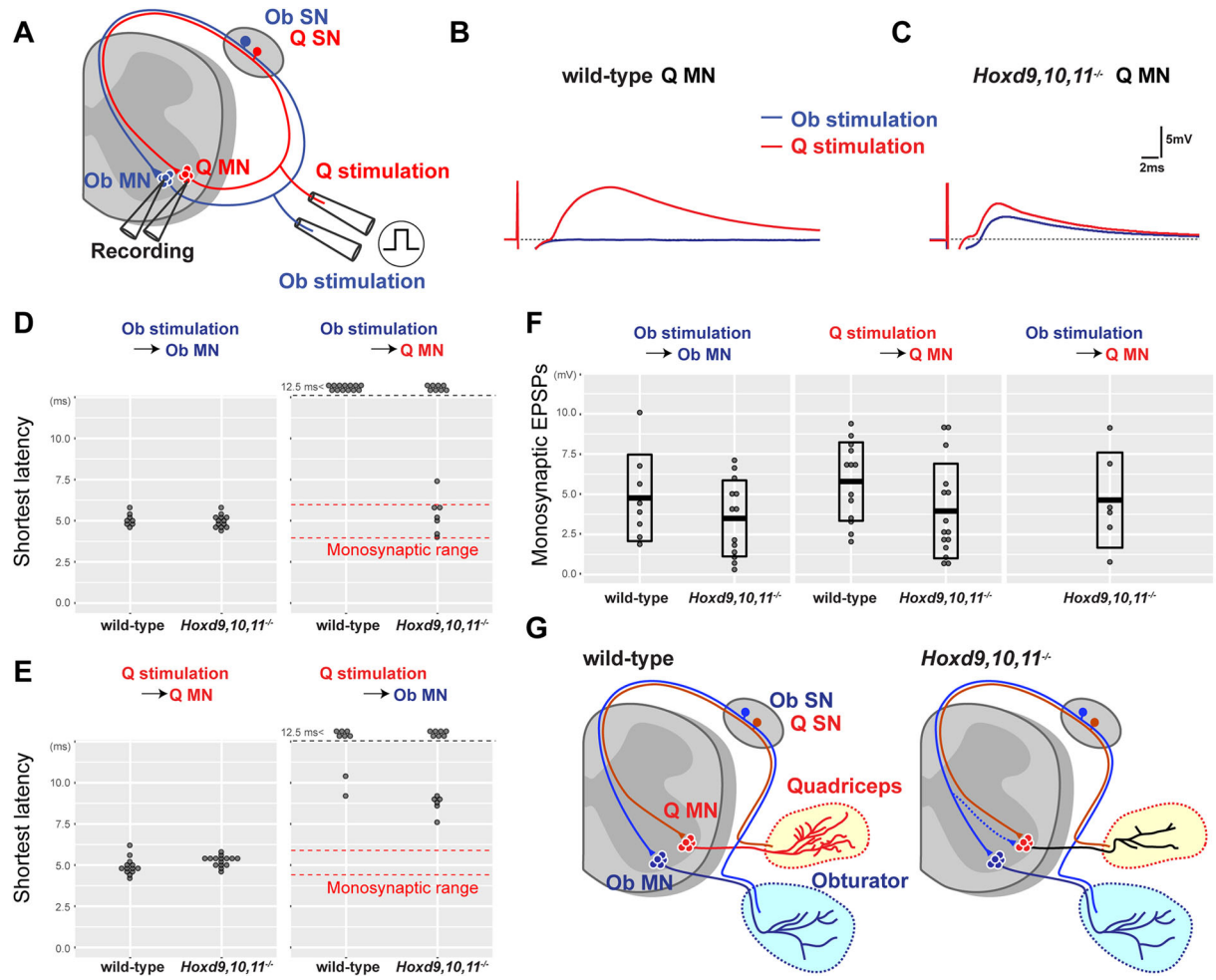

Fig. 3. Loss of HoxD9, HoxD10 and HoxD11 disturbs synaptic specificities between quadriceps and obturator reflex arc. (A) Schematic of the intracellular recording experiment for examining sensory-motor connectivity. Obturator (Ob, blue) and quadriceps (Q, red) motor neurons (MNs) were identified by antidromic responses from obturator and quadriceps sensory nerve (SN) stimulation (Ob and Q stimulation), respectively. (B,C) Individual traces of quadriceps motor neurons with obturator stimulation (blue) or quadriceps stimulation (red) from wild-type (B) and *Hoxd9, 10, 11*$^{-/-}$ (C) mice. (D,E) Quantification of the shortest excitatory postsynaptic potential (EPSP) onset latencies from recordings of individual motor neurons with obturator stimulation (D) and quadriceps stimulation (E). Monosynaptic ranges (red dashed lines) were defined by homonymous connections (recordings of obturator motor neurons with obturator nerve stimulation or recordings of quadriceps motor neurons with quadriceps nerve stimulation). Wild-type data: quadriceps: *n*=13, obturator: *n*=8, from three mice. *Hoxd9, 10, 11*$^{-/-}$ mouse data: quadriceps: *n*=15, obturator: *n*=13, from eight mice. (F) Dot plots of peak amplitudes of homonymous monosynaptic EPSPs (left, middle) and aberrant EPSPs (right). Box plots show mean values (middle bars) and s.d. ranges (boxes). (G) Schematic summary of sensory-motor connectivity differences observed in wild-type and *Hoxd9, 10, 11*$^{-/-}$ mice. Ob and Q MNs received monosynaptic inputs from Ob and Q SNs, respectively (left). In the absence of HoxD9, 10 and 11 (right), Q MNs have thinner and less branched axons (black) and receive aberrant inputs from Ob sensory axons (blue dotted line).

Retrograde labeling of motor neurons by AAV

To label motor neurons (Fig. 2), AAV6-CAG-tdTomato (4.5×10^{12} vg/ml, 1 µl, UNC Vector Core) was injected into quadriceps or gracilis muscles at P3 and mice were sacrificed at P10.

Tissue preparation

Spinal cords, DRGs and the surrounding tissues were fixed with 4% paraformaldehyde (PFA)/phosphate buffer (PB) for 20 min (embryos) or overnight (postnatal mice) for immunostaining or *in situ* hybridization. Samples were then cryoprotected in 30% sucrose, embedded in OCT compound and sectioned with a cryostat (Leica VT1200) at a thickness of 16 µm. For analyses of motor neuron cell body positions and dendrite projections, spinal cords were embedded in 4% low-melting agarose then sectioned into 200 µm slices using a vibratome (Leica CM1860).

In situ hybridization

Digoxigenin (DIG)-labeled RNA probes were synthesized using a DIG labeling kit (Roche). *In situ* hybridization was performed according to standard protocols (Schaeren-Wiemers and Gerfin-Moser, 1993).

Immunostaining and scanning

The following antibodies were used in this study: rabbit anti-Hoxd10 (ab76897, Abcam, 1/200), goat anti-Islet1 (AF1837, R&D Systems, 1/50), rabbit anti-nNOS (#24287, Immunostar, 1/1000), goat anti-FoxP1 (AF4534, R&D Systems, 1/100) and rabbit anti-Pea3 (kindly provided by Dr Silvia Arber, University of Basel, Switzerland, 1/20,000). Sections were stained with Alexa488 or Alexa568-conjugated secondary antibodies (A21206, A110042, A11055, A11057, Thermo Fisher Scientific, 1/500), then mounted with Vectashield (Vector Laboratories). To analyze motor axon projections in muscles, embryos were fixed and cleared using SeeDB or CUBIC (Ke et al., 2013; Kubota et al., 2017). Vibratome sections (200 µm) were treated with CUBIC-L (T3740, TCI America) at 37°C for 30 min, then sections were treated with 50% then 100% CUBIC-R+ (T3741, TCI America) for final clearing. Samples were scanned using Nikon A1R and Leica SP8 confocal microscopes.

Intracellular recordings

Dissection of spinal cords and intracellular recordings were performed as previously described (Imai et al., 2016a,b). Briefly, after perfusion, spinal

Development (2021) 148, dev191122. doi:10.1242/dev.191122

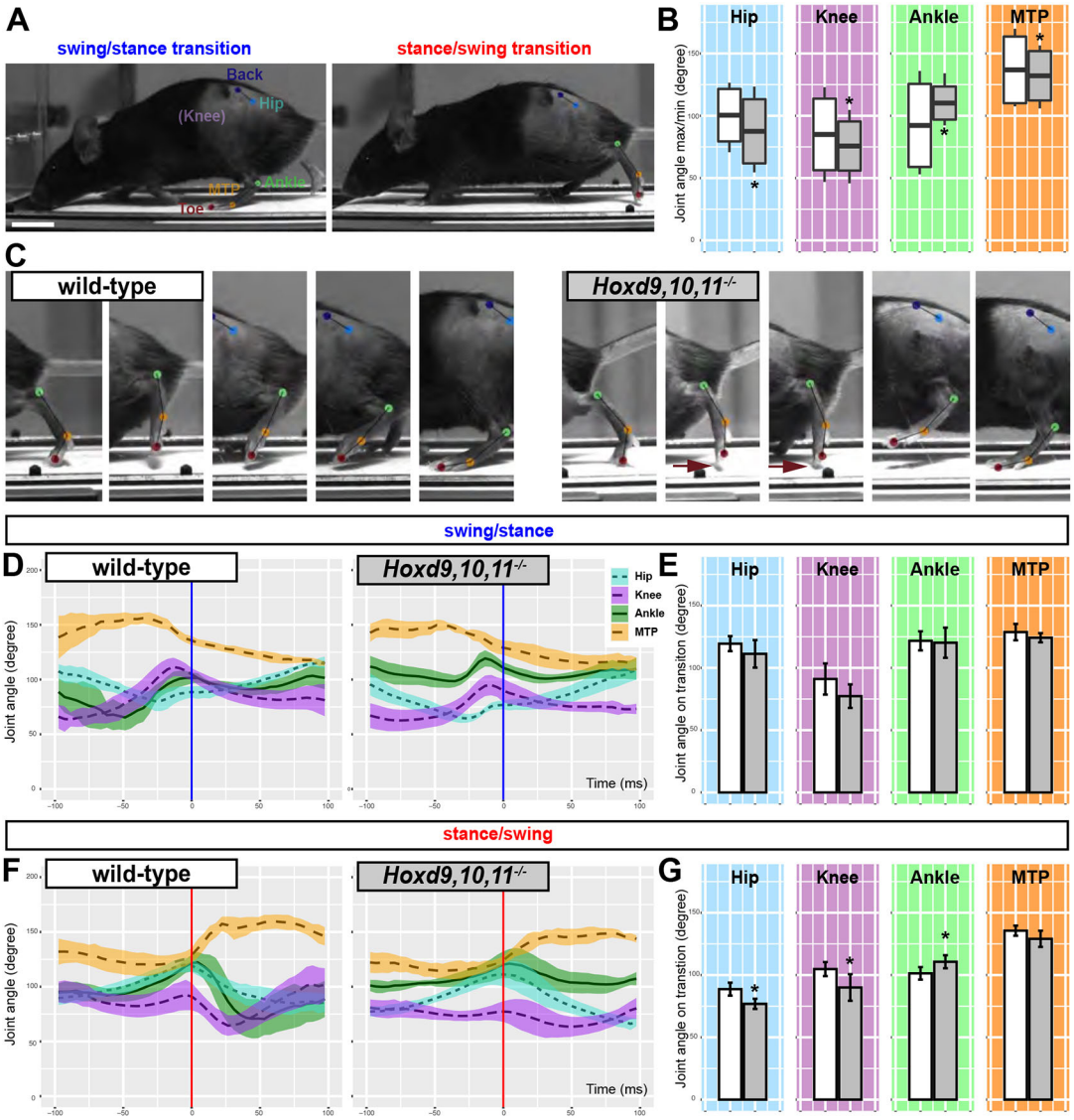

Fig. 4. *Hoxd9, 10, 11*$^{-/-}$ mice exhibit defects in locomotion. (A) Backs, hips, ankles, metatarsal phalangeal joints (MTPs) and toes of mice were marked and recorded during locomotion (25 cm/s). Panels show swing/stance (left) and stance/swing transition phases (right). (B) Quantification of the range (maximum and minimal joint angles) of hip, knee, ankle and MTP for wild-type (white, *n*=5) and *Hoxd9, 10, 11*$^{-/-}$ (grey, *n*=5) mice during locomotion. (C) Representative frames (every 22.1 ms) during locomotion of wild-type (left) and *Hoxd9, 10, 11*$^{-/-}$ mice (right). Red arrows indicate foot-dragging behavior in mutants. (D-G) Differences in joint flexion during transitions between swing/stance (D) and stance/swing phases (F) in wild-type and *Hoxd9, 10, 11*$^{-/-}$ mice. Comparison of joint angles at the mid-point between swing/stance (E, blue lines in D) and stance/swing (G, red lines in F) phases. All data are mean±s.d. **P*<0.05 (unpaired two-tailed Student's *t*-test). Scale bar: 1 cm (A).

cords from P5-P7 pups were removed and hemi-sectioned in an oxygenated cerebrospinal fluid (aCSF) bath containing NaCl (127 mM), KCl (1.9 mM), KH_2PO_4 (1.2 mM), $CaCl_2$ (2 mM), $MgSO_4$ (1 mM), $NaHCO_3$ (26 mM) and D-glucose (20.5 mM). Using tightly-fitting glass pipettes, obturator and quadriceps nerves were stimulated independently (10 mA, S88X, SIU-C Grass Technologies). Intracellular potentials were recorded using glass micropipettes (90-180 MΩ) filled with 2 M potassium acetate with 0.5% Fast Green and 300 mM of lidocaine N-ethyl bromide for blocking antidromic potentials (Sigma-Aldrich). Synaptic potentials evoked by 1 Hz stimulation of either the quadriceps or obturator nerves were recorded 20-60 times and then averaged (MultiClamp 700B, Digidata 1440A, Clampex 10, Molecular Devices). Obturator and quadriceps motor neurons were identified by antidromic activation. Recordings were accepted only from neurons in which the resting membrane potential was below −40 mV (Mears and Frank, 1997). The time window for monosynaptic EPSP onset latencies was defined as the mean latency of wild-type homonymous EPSPs±2 s.d., as previously described (Vrieseling and Arber, 2006; Pecho-Vrieseling et al., 2009; Fukuhara et al., 2013).

Quantification and statistical analysis

For counting motor neurons (Fig. 1), every fourth section (thickness: 16 µm) was labeled, scanned and counted using ImageJ software. Motor neuron morphologies (Fig. 2) were analyzed with surface tools in the IMARIS software package (Bitplane). For motor neuron cell body density analyses (Fig. 2), bin sizes were set to 100 µm. The densities of motor neuron dendrite projections (Fig. 2) were evaluated in 30° bins using ImageJ software. For quantifications of quadriceps and obturator motor axons (Fig. 2), volumes were analyzed with surface tools in IMARIS software (quadriceps: wild-type, 3,106,551±800,904 µm^3, mutants, 1,231,847 ±496,490 µm^3; obturator: wild-type, 3,061,520±326,758 µm^3, mutants, 3,024,534±421,486 µm^3). For joint angle analyses (Fig. 4), swing/stance and stance/swing transition phases were manually defined, then analyzed,

averaged (10-15 cycles) and compared using an unpaired two-tailed Student's *t*-test.

Acknowledgements
We are grateful to Silvia Arber (University of Basel) for providing us with the Pea3 antibody. We also thank David Ladle (Wright State University), Turgay Akay (Dalhousie University), Joriene De Nooij (Columbia University) and Niccolo Zampieri (Max-Delbrück-Center for Molecular Medicine Berlin-Buch) for critically reading this manuscript.

Competing interests
The authors declare no competing or financial interests.

Author contributions
Conceptualization: Y.Y., F.I., S.S.P.; Methodology: F.I., S.S.P.; Validation: F.I.; Formal analysis: F.I.; Investigation: F.I.; Resources: S.S.P., M.A.; Data curation: F.I.; Writing - original draft: F.I.; Writing - review & editing: Y.Y., S.S.P.; Supervision: Y.Y., S.S.P.; Funding acquisition: Y.Y.

Funding
This work was supported by the National Institute of Neurological Disorders and Stroke (NS100772, NS093002, NS115963 and NS093002). Deposited in PMC for release after 12 months.

Peer review history
The peer review history is available online at https://journals.biologists.com/dev/article-lookup/doi/10.1242/dev.191122

References

Akay, T. (2020). Sensory feedback control of locomotor pattern generation in cats and mice. *Neuroscience* **450**, 161-167. doi:10.1016/j.neuroscience.2020.05.008

Akay, T., Tourtellotte, W. G., Arber, S. and Jessell, T. M. (2014). Degradation of mouse locomotor pattern in the absence of proprioceptive sensory feedback. *Proc. Natl. Acad. Sci. USA* **111**, 16877-16882. doi:10.1073/pnas.1419045111

Arber, S. (2012). Motor circuits in action: specification, connectivity, and function. *Neuron* **74**, 975-989. doi:10.1016/j.neuron.2012.05.011

Arber, S., Ladle, D. R., Lin, J. H., Frank, E. and Jessell, T. M. (2000). ETS gene Er81 controls the formation of functional connections between group Ia sensory afferents and motor neurons. *Cell* **101**, 485-498. doi:10.1016/S0092-8674(00)80859-4

Baek, M., Pivetta, C., Liu, J.-P., Arber, S. and Dasen, J. S. (2017). Columnar-intrinsic cues shape premotor input specificity in locomotor circuits. *Cell Rep.* **21**, 867-877. doi:10.1016/j.celrep.2017.10.004

Baek, M., Menon, V., Jessell, T. M., Hantman, A. W. and Dasen, J. S. (2019). Molecular logic of spinocerebellar tract neuron diversity and connectivity. *Cell Rep.* **27**, 2620-2635.e2624. doi:10.1016/j.celrep.2019.04.113

Balaskas, N., Ng, D. and Zampieri, N. (2020). The positional logic of sensory-motor reflex circuit assembly. *Neuroscience* **450**, 142-150. doi:10.1016/j.neuroscience.2020.04.038

Balaskas, N., Abbott, L. F., Jessell, T. M. and Ng, D. (2019). Positional strategies for connection specificity and synaptic organization in spinal sensory-motor circuits. *Neuron* **102**, 1143-1156. e1144. doi:10.1016/j.neuron.2019.04.008

Carpenter, E. M., Goddard, J. M., Davis, A. P., Nguyen, T. P. and Capecchi, M. R. (1997). Targeted disruption of Hoxd-10 affects mouse hindlimb development. *Development* **124**, 4505-4514. doi:10.1242/dev.124.22.4505

Catela, C., Shin, M. M. and Dasen, J. S. (2015). Assembly and function of spinal circuits for motor control. *Annu. Rev. Cell Dev. Biol.* **31**, 669-698. doi:10.1146/annurev-cellbio-100814-125155

Choe, A., Phun, H. Q., Tieu, D. D., Hu, Y. H. and Carpenter, E. M. (2006). Expression patterns of Hox10 paralogous genes during lumbar spinal cord development. *Gene Expr. Patterns* **6**, 730-737. doi:10.1016/j.modgep.2005.12.004

Dasen, J. S. and Jessell, T. M. (2009). Hox networks and the origins of motor neuron diversity. *Curr. Top. Dev. Biol.* **88**, 169-200. doi:10.1016/S0070-2153(09)88006-X

Davis, A. P. and Capecchi, M. R. (1994). Axial homeosis and appendicular skeleton defects in mice with a targeted disruption of hoxd-11. *Development* **120**, 2187-2198. doi:10.1242/dev.120.8.2187

de la Cruz, C. C., Der-Avakian, A., Spyropoulos, D. D., Tieu, D. D. and Carpenter, E. M. (1999). Targeted disruption of Hoxd9 and Hoxd10 alters locomotor behavior, vertebral identity, and peripheral nervous system development. *Dev. Biol.* **216**, 595-610. doi:10.1006/dbio.1999.9528

De Marco Garcia, N. V. and Jessell, T. M. (2008). Early motor neuron pool identity and muscle nerve trajectory defined by postmitotic restrictions in Nkx6.1 activity. *Neuron* **57**, 217-231. doi:10.1016/j.neuron.2007.11.033

Frank, E. (1990). The formation of specific synaptic connections between muscle sensory and motor neurons in the absence of coordinated patterns of muscle activity. *J. Neurosci.* **10**, 2250-2260. doi:10.1523/JNEUROSCI.10-07-02250.1990

Fukuhara, K., Imai, F., Ladle, D. R., Katayama, K., Leslie, J. R., Arber, S., Jessell, T. M. and Yoshida, Y. (2013). Specificity of monosynaptic sensory-motor connections imposed by repellent Sema3E-PlexinD1 signaling. *Cell Rep.* **5**, 748-758. doi:10.1016/j.celrep.2013.10.005

Haase, G., Dessaud, E., Garces, A., de Bovis, B., Birling, M., Filippi, P., Schmalbruch, H., Arber, S. and deLapeyrière, O. (2002). GDNF acts through PEA3 to regulate cell body positioning and muscle innervation of specific motor neuron pools. *Neuron* **35**, 893-905. doi:10.1016/S0896-6273(02)00864-4

Imai, F. and Yoshida, Y. (2018). Molecular mechanisms underlying monosynaptic sensory-motor circuit development in the spinal cord. *Dev. Dyn.* **247**, 581-587. doi:10.1002/dvdy.24611

Imai, F., Chen, X., Weirauch, M. T. and Yoshida, Y. (2016a). Requirement for dicer in maintenance of monosynaptic sensory-motor circuits in the spinal cord. *Cell Rep.* **17**, 2163-2172. doi:10.1016/j.celrep.2016.10.083

Imai, F., Ladle, D. R., Leslie, J. R., Duan, X., Rizvi, T. A., Ciraolo, G. M., Zheng, Y. and Yoshida, Y. (2016b). Synapse formation in monosynaptic sensory-motor connections is regulated by presynaptic Rho GTPase Cdc42. *J. Neurosci.* **36**, 5724-5735. doi:10.1523/JNEUROSCI.2146-15.2016

Jung, H., Lacombe, J., Mazzoni, E. O., Liem, K. F., Jr, Grinstein, J., Mahony, S., Mukhopadhyay, D., Gifford, D. K., Young, R. A., Anderson, K. V. et al. (2010). Global control of motor neuron topography mediated by the repressive actions of a single hox gene. *Neuron* **67**, 781-796. doi:10.1016/j.neuron.2010.08.008

Ke, M.-T., Fujimoto, S. and Imai, T. (2013). SeeDB: a simple and morphology-preserving optical clearing agent for neuronal circuit reconstruction. *Nat. Neurosci.* **16**, 1154-1161. doi:10.1038/nn.3447

Kubota, S. I., Takahashi, K., Nishida, J., Morishita, Y., Ehata, S., Tainaka, K., Miyazono, K. and Ueda, H. R. (2017). Whole-body profiling of cancer metastasis with single-cell resolution. *Cell Rep.* **20**, 236-250. doi:10.1016/j.celrep.2017.06.010

Lacombe, J., Hanley, O., Jung, H., Philippidou, P., Surmeli, G., Grinstein, J. and Dasen, J. S. (2013). Genetic and functional modularity of Hox activities in the specification of limb-innervating motor neurons. *PLoS Genet.* **9**, e1003184. doi:10.1371/journal.pgen.1003184

Ladle, D. R., Pecho-Vrieseling, E. and Arber, S. (2007). Assembly of motor circuits in the spinal cord: driven to function by genetic and experience-dependent mechanisms. *Neuron* **56**, 270-283. doi:10.1016/j.neuron.2007.09.026

Mathis, A., Mamidanna, P., Cury, K. M., Abe, T., Murthy, V. N., Mathis, M. W. and Bethge, M. (2018). DeepLabCut: markerless pose estimation of user-defined body parts with deep learning. *Nat. Neurosci.* **21**, 1281-1289. doi:10.1038/s41593-018-0209-y

Mayer, W. P., Murray, A. J., Brenner-Morton, S., Jessell, T. M., Tourtellotte, W. G. and Akay, T. (2018). Role of muscle spindle feedback in regulating muscle activity strength during walking at different speed in mice. *J. Neurophysiol.* **120**, 2484-2497. doi:10.1152/jn.00250.2018

Mears, S. C. and Frank, E. (1997). Formation of specific monosynaptic connections between muscle spindle afferents and motoneurons in the mouse. *J. Neurosci.* **17**, 3128-3135. doi:10.1523/JNEUROSCI.17-09-03128.1997

Mendelsohn, A. I., Simon, C. M., Abbott, L. F., Mentis, G. Z. and Jessell, T. M. (2015). Activity regulates the incidence of heteronymous sensory-motor connections. *Neuron* **87**, 111-123. doi:10.1016/j.neuron.2015.05.045

Mendelson, B. and Frank, E. (1991). Specific monosynaptic sensory-motor connections form in the absence of patterned neural activity and motoneuronal cell death. *J. Neurosci.* **11**, 1390-1403. doi:10.1523/JNEUROSCI.11-05-01390.1991

Nath, T., Mathis, A., Chen, A. C., Patel, A., Bethge, M. and Mathis, M. W. (2019). Using DeepLabCut for 3D markerless pose estimation across species and behaviors. *Nat. Protoc.* **14**, 2152-2176. doi:10.1038/s41596-019-0176-0

Pecho-Vrieseling, E., Sigrist, M., Yoshida, Y., Jessell, T. M. and Arber, S. (2009). Specificity of sensory-motor connections encoded by Sema3e-Plxnd1 recognition. *Nature* **459**, 842-846. doi:10.1038/nature08000

Philippidou, P. and Dasen, J. S. (2013). Hox genes: choreographers in neural development, architects of circuit organization. *Neuron* **80**, 12-34. doi:10.1016/j.neuron.2013.09.020

Raines, A. M., Adam, M., Magella, B., Meyer, S. E., Grimes, H. L., Dey, S. K. and Potter, S. S. (2013). Recombineering-based dissection of flanking and paralogous Hox gene functions in mouse reproductive tracts. *Development* **140**, 2942-2952. doi:10.1242/dev.092569

Raines, A. M., Magella, B., Adam, M. and Potter, S. S. (2015). Key pathways regulated by HoxA9,10,11/HoxD9,10,11 during limb development. *BMC Dev. Biol.* **15**, 28. doi:10.1186/s12861-015-0078-5

Santuz, A., Akay, T., Mayer, W. P., Wells, T. L., Schroll, A. and Arampatzis, A. (2019). Modular organization of murine locomotor pattern in the presence and absence of sensory feedback from muscle spindles. *J. Physiol.* **597**, 3147-3165. doi:10.1113/JP277515

Schaeren-Wiemers, N. and Gerfin-Moser, A. (1993). A single protocol to detect transcripts of various types and expression levels in neural tissue and cultured cells: in situ hybridization using digoxigenin-labelled cRNA probes. *Histochemistry* **100**, 431-440. doi:10.1007/BF00267823

Shin, M. M., Catela, C. and Dasen, J. (2020). Intrinsic control of neuronal diversity and synaptic specificity in a proprioceptive circuit. *eLife* **9**, e56374. doi:10.7554/eLife.56374

Sürmeli, G., Akay, T., Ippolito, G. C., Tucker, P. W. and Jessell, T. M. (2011). Patterns of spinal sensory-motor connectivity prescribed by a dorsoventral positional template. *Cell* **147**, 653-665. doi:10.1016/j.cell.2011.10.012

Sweeney, L. B., Bikoff, J. B., Gabitto, M. I., Brenner-Morton, S., Baek, M., Yang, J. H., Tabak, E. G., Dasen, J. S., Kintner, C. R. and Jessell, T. M. (2018). Origin and Segmental Diversity of Spinal Inhibitory Interneurons. *Neuron* **97**, 341-355.e343. doi:10.1016/j.neuron.2017.12.029

Tschopp, P., Christen, A. J. and Duboule, D. (2012). Bimodal control of Hoxd gene transcription in the spinal cord defines two regulatory subclusters. *Development* **139**, 929-939. doi:10.1242/dev.076794

Vrieseling, E. and Arber, S. (2006). Target-induced transcriptional control of dendritic patterning and connectivity in motor neurons by the ETS gene Pea3. *Cell* **127**, 1439-1452. doi:10.1016/j.cell.2006.10.042

Wang, Z., Li, L. Y., Taylor, M. D., Wright, D. E. and Frank, E. (2007). Prenatal exposure to elevated NT3 disrupts synaptic selectivity in the spinal cord. *J. Neurosci.* **27**, 3686-3694. doi:10.1523/JNEUROSCI.0197-07.2007

Wichterle, H., Lieberam, I., Porter, J. A. and Jessell, T. M. (2002). Directed differentiation of embryonic stem cells into motor neurons. *Cell* **110**, 385-397. doi:10.1016/S0092-8674(02)00835-8

Wu, Y., Wang, G., Scott, S. A. and Capecchi, M. R. (2008). Hoxc10 and Hoxd10 regulate mouse columnar, divisional and motor pool identity of lumbar motoneurons. *Development* **135**, 171-182. doi:10.1242/dev.009225

Zampieri, N. and Nooij, J. D. (2021). Regulating muscle spindle and Golgi tendon organ proprioceptorphenotype. *Curr. Opin. Physiol.* **19**, 204-210. doi:10.1016/j.cophys.2020.11.001

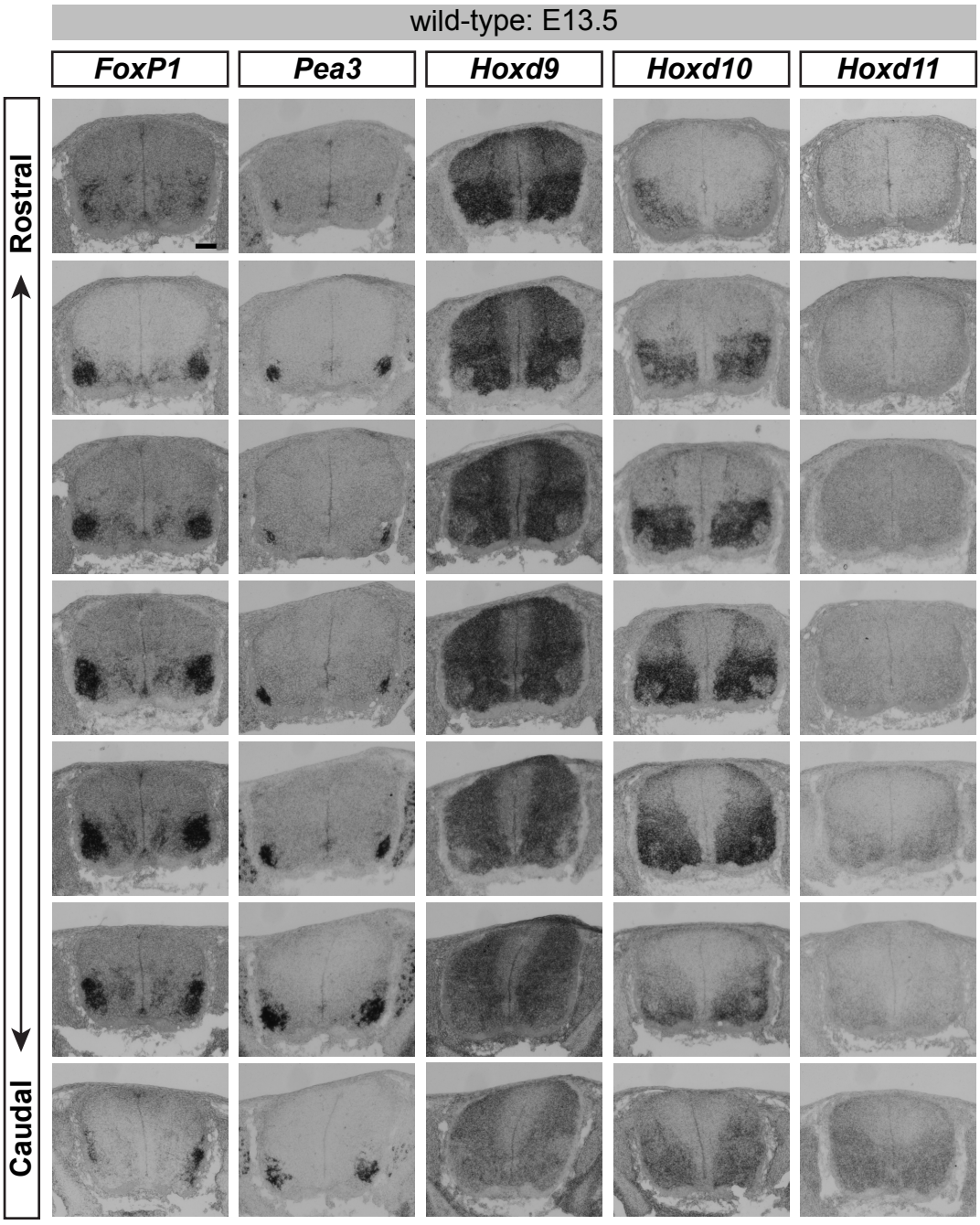

Figure S1. Gene expression patterns of Hoxd genes
Foxp1, *Pea3*, *Hoxd9*, *Hoxd10* and *Hoxd11* expression in the lumbar spinal cord of wild-type embryos at E13.5. Scale bar: 100μm.